ASPECTS OF CEMENT STABILIZED MOZAMBIQUE SAND BASE MATERIAL PERFORMANCE UNDER MMLS3 AND MLS10 APT TRAFFICKING

Fred Hugo[1], Eben.R. de Vos[2] and Hilário Tayob[3]

[1]Director, Institute for Transport Technology, University of Stellenbosch
Stellenbosch, South Africa 7600
Tel. +27 21 808-4364 Fax.+27 21 808-4361; Email: fhugo@sun.ac.za
[2]Researcher, Institute for Transport Technology, University of Stellenbosch
Private Bag X1, Stellenbosch, South Africa 7600
Tel. +27 21 808-4079 Fax.+27 21 808-4361; Email: erdevos@sun.ac.za
[3]ANE Project coordinator, National Administration of roads
Directorate of National Roads, Engineering Department
Av. de Moçambique 1225, C.P. 1439, Maputo - Mozambique
Phones +25821476163/7 - Fax +25821475862 ; Email : htayob@ane.gov.mz

ABSTRACT

The World Bank sponsored research to support preservation and maintenance efforts in Mozambique. The object was to develop guidelines for a mechanistic-empirical design method for cement stabilized sand bases (CTB) in Mozambique using Accelerated Pavement Testing (APT) technology. APT encompassed scaled (one third) and full-scale APT using mobile load simulator technology (MMLS3 and MLS10). The MLS10 expanded the MMLS3 APT investigation to full-scale pavements, including wet trafficking cycles to emulate environmental effects. Operation of the MLS10 is similar to the MMLS3. It has four sets of dual wheels running in a closed loop with a maximum speed of up to 22 kph. Loads of 60kN and 70kN were used for trafficking. Fifteen MMLS3 tests and six full-scale test sections were tested. Comparative results between MMLS3 tests and full-scale MLS10 tests were found. Distress mechanisms were similar. Related design features and material strength parameters were used as supplementary and verification tools.

INTRODUCTION

The World Bank sponsored this research project to support preservation and maintenance efforts in Mozambique. The object was to develop guidelines for a mechanistic-empirical pavement design method for cement stabilized sand bases (CTB) based on Accelerated Pavement Testing (APT) technology. The APT program encompassed both scaled (one third) and full-scale APT using mobile load simulator technology (MMLS3 and MLS10).

The scope of the paper is limited to a presentation of aspects of Mozambique CTB material performance under the APT trafficking. The APT was focused on three primary phases:

- Exploratory scaled laboratory MMLS3 testing
- Construction of field test sections
- Full-scale and scaled field APT by means of MLS10 and MMLS3

The MMLS3 was used to evaluate the performance of the stabilized coastal sands under different trafficking conditions in the laboratory. This was to serve for identifying potential failure mechanisms for comparison with failure mechanisms observed in the field. In similar vein, this information was to provide the basis for formulation of the specifications for constructing full scale test sections to be tested by the MMLS3 and the MLS10. It was also used as input for the mechanistic modelling. Fifteen MMLS3 tests, including two field tests were completed as well as six full-scale MLS10 tests.

SCALED LABORATORY TESTING PROGRAM

The most commonly and abundent material used by local consultants namely, the reddish and yellowish coloured sands were used in this study. The sands were evaluated in terms of performance under MMLS3 APT as well as their physical, chemical and strength charactistics through supplementary and verification testing (S/VT).

Two binder types were selected for stabilisation namely, cement and a fifty percent cement-lime blend. This decision was based on past and current practise of using cement, as well as exploration of performance of a possible alternative namely, a blend of cement and lime. These two binder types were used for the construction of the scaled and full-scale test sections as well as specimen preparation for material strength testing.

The test load characteristics of the MMLS3 are summarised in Table 1 together with the load characteristics of the MLS10. The findings of the MMLS3 tests are summarized in Table 2. A set-up view of the MLS10 trafficking on the test site at Manhiça in Mozambique is shown in Figures 1.

The results from the laboratory and field MMLS3 tests enabled:

- Comparison of the relative performance of the stabilising agents.
- Understanding the manifested distress mechanisms
- Adjudicating the expected pavement performance in order to predict/estimate the full-scale performance characteristics of the test sections

Both the red and yellow coastal sands performed well after stabilizing with five percent cement or a blend of 5% blend of cement and lime (ratio 50:50). The load applications were respectively 1.3 and 1.4 million. The relationship of these axles to the full-scale MLS10 is discussed later. The seven percent sections withstood trafficking in excess of three million axle load applications.

Environmental trafficking conditions were simulated by:

- initially trafficking at ambient temperature for 50k followed by
- alternate heated trafficking at 50C at 20mm depth for the next 200k and
- 50k wet trafficking cycles at ambient temperature with water sprayed on the pavement surface.

Figure 1: Set-up view of the MLS10 trafficking on the test site at Manhiça in Mozambique

Table1: Comparison of MMLS3 and MLS10 APT Machine Parameters and Load Characteristics

	Item		1/3 Scale MMLS3	Standard MLS10
1	Testing length	m	1	4
2	Tread path width	mm	80	610
3	Size of test section	m	1 x 0.4 (min)	5m x 1.6
4	Wheel configuration		Single	Single/Dual
5	Wheel load	kN	1.9 - 2.9	30 - 75
6	Wheel suspension		Spring	Pneumatic Hydraulic
7	Wheel velocity	m/s	2.5	7.2
8	Load propulsion		Electric Drum drive	Linear Induction Motors (LIM)
9	Power		Electric	Electric - On board generator
10	Power consumption	kW	1.5	140 max
11	Temperature control		Yes (Hot and Cold)	Heating feasible
12	Trolley description		Four bogies with spring suspension	Four bogies with pneumatic hydraulic suspension
13	Data acquisition system		Digital	Digital (Electrical – delete)
14	Load control		Mechanical	Pneumatic Hydraulic
15	Mass	ton	0.7	29
16	Data acquisition		Flexible per design	Flexible per design
17	Vehicle dimensions	L*B*H	2.5 x 0.7 x 1.2	10.7 x 2.4 x 3.1 (can raise 1 meter for access below)
18	No of wheels		4	4 dual / super single
19	Tyres		Vredestein 6 ply pneumatic	Continental R22.5 295/65 ; super single 385/65
20	Tyre pressure	kPa	400 - 800	500 - 1000
21	Speed of operation	Kph	8.7 simulating 26	26
22	Rut depth (max)	mm	10	50
23	Repetition /h		7200	7200 max 6000 operational
24	Trafficking conditions		Dry, heated, wet heated	Dry/Wet Heated
25	Trafficked width	mm	80 - 240	610 – 1 600 (optional)
26	Lateral Traffic Load Distribution	mm	Gaussian or channelised +/- 80	Gaussian or channelised Programmable +/- 500
27	Lifting mechanism(s)		Screw jacks	Automated hydraulic jacks
28	Lateral displacement		Electric motor	Automated hydraulic jacks
29	Short haul mobility		Hand drawn	Hydraulic motor
30	Long haul mobility		Trailer	Low bed trailer/container

Table2: MMLS3 test results with laboratory and field trafficking

MATERIAL TYPE	STABILISING AGENT	SURF-ACING	AXLES TO FAILURE	DISTRESS MECHANISMS
Red	3 % CEM II 32.5	HMA	150 000	·Pumping >>Crushing ·Horizontal & vertical shear ·Flexural cracking ·Interface distress
Red	3 % CEM II 32.5	SEAL	145 000	·Shear followed by bottom-up cracking to neutral axis
Red	7 % CEM II 32.5 + 1.5 % Lime (ILC)	HMA	3 100 000	·Local distress induced by artificial transverse cracking ·Longitudinal flexural cracks (longitudinal growth)
Red	3.5% CEM II 32.5 + 3.5 % Lime +1.5 % ILC	HMA	3 100 000	·Transverse cracks ·Longitudinal flexural cracks
Red	7 % CEM II 32.5+ 1.5 % ILC	SEAL	3 500 000	·No apparent distress @ 2.9 m
Red	5% CEM II 32.5	HMA	1 300 000	·Long and transverse cracking ·Ageing had an important effect
Red	2.5 % CEM II 32.5 + 2.5% Lime	HMA	1 400 000	·Longitudinal flexural crack ·Secondary transverse cracking
Yellow	7 % CEM II 32.5 +	HMA	2 400 000	·No apparent distress
Red Drilled cores reconstituted	5 % CEM II 32.5	SEAL	125 000	Longitudinal flexural cracking - Interface distress
Red Field	1.5 % CEM II 32.5 + 4.0% SS60	SEAL	200 000* Field test	·Rutting ·Secondary cracking
Red Field	5.5% SS60	SEAL	19 000* Field test	·Rutting ·Seal failed due to debonding and interface distress
Red Field	1.5 % CEM II 32.5 + 4.0% SS60	SEAL	200 000* Field test	·Rutting ·Secondary cracking
Red Field	5.5% SS60	SEAL	80 000*	·Rutting ·Seal failed due to debonding and interface distress
Red Field	5 % CEM II 32.5	SEAL	1 700 000* Field test	·No debonding

UNDERSTANDING THE MANIFESTED DISTRESS MECHANISMS UNDER MMLS3 TRAFFICKING

The performance of the cement-lime blend was in general better than the plain Portland cement in terms of MMLS3 trafficking and loss- of-stiffness. Distress mechanisms were explored by dissecting extracted specimens from the pavement. Crack patterns and rupture planes were mapped. Micro-cracks, were tracked as well as the manner and sequence in which distress occurred. The performance was found from the tests in the laboratory and in the field:

- Surface distress under the asphalt surfacing is evident. The distress is aggravated when water ingresses during trafficking. The extent of damage is related to the extent to which water can infiltrate. Stiffness ratios (relating the stiffness after trafficking to that before) as low as 0.50 were found where the surface of the structure had been pulverised and sand was being pumped out during trafficking.
- Horizontal shear at the interface between the asphalt surfacing and the underlying CTB occurs during trafficking of thin asphaltic surfacing (seal and HMA) when the CTB has a low strength (3 % cement content). This leads to delamination at spots resulting in the erosion of the underlying CTB. Sections containing 5% cement content maintained the bond better than the 3 % sections.
- Pumping of the CTB material occurs when the CTB surface becomes pulverised or crushed. The pumping appears to be initiated by water infiltrating through cracks in the asphalt.
- Longitudinal cracking in the CTB was found in the scaled pavements and in the full-scale test pavements (as well as the cores that were tested in the test bed). This phenomenon was also observed on old and new sections of highway EN1, where such cracks had migrated to the pavement surface.
- The P-SPA was successful in monitoring degradation of the pavement structure. It yielded stiffness results in terms of the ratio between trafficked and untrafficked response that reflected the state of the in-situ pavement. As distress and failure increased the ratio progressively reduced.
- The worst damage appeared in the locations with the highest in-situ moisture content, evidence of the major impact of water ingress.
- Surface rutting appeared to be related to densification of the asphalt and pulverising and/or crushing of the CTB. No densification of the sand subbase subgrade was evident.
- The 7% yellow sand performed very much the same as the red sand under trafficking.

In summary the degradation process consisted of the follow mechanisms:

- ♦ Bottom up longitudinal cracking
- ♦ Transverse cracking
- ♦ Horizontal shear plane formation in the middle of the combined CTB and HMA pavement structure
- ♦ CTB/HMA interface distress in the low cement content sections.

The order and direction of development of cracks was dependent on structural composition, material properties and construction history. A comparison of MMLS3 failure mechanisms with those found under MLS10 trafficking is discussed later. It is note worthy that the trends in relative seismic stiffness ratio under MMLS3 and MLS10 trafficking in the laboratory and the in the field respectively are similar in nature (see Figure 2).

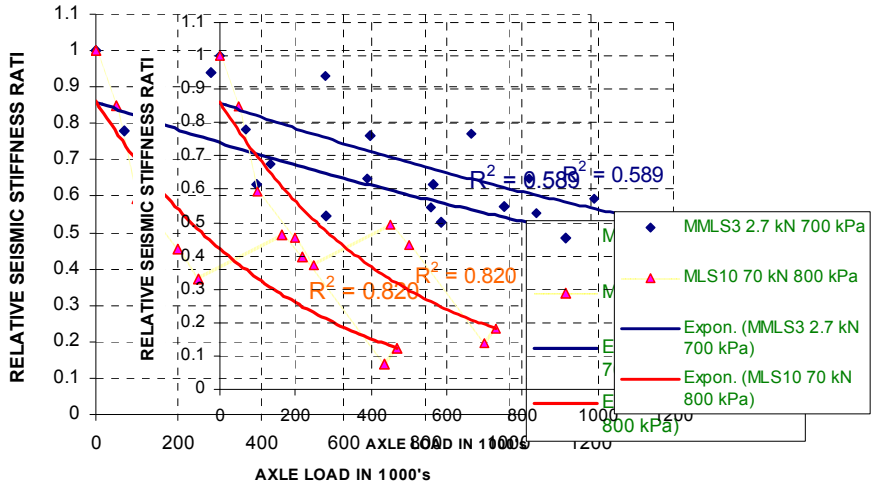

Figure 2: Relative stiffness ratios for MMLS3 and MLS10 – 7% CTB in lab and field

SUPPLEMENTARY AND VERIFICATION TESTING (S/VT)

Testing comprised exploration of physical, chemical and strength charactistics.

Physical and chemical characteristics of sands

Engineering properties normally determined on site or central laboratories could not identify a significant difference in the properties of reddish or yellowish coloured sands. Electron microscope analyses were conducted by Energy Dispersive Spectroscopy (EDS) in the geology department of the University of Stellenbosch. The photos were taken with back scatter detector which shows differences in chemistry in shades of grey on polished slide sections. Differences in coatings can be seen.

The findings yielded a number of differences in the characteristics of the two sands.

1. Particle sizes differed:
    a. Yellow sand - single sized and larger particles
    b. Red sand - smaller in size with some apparent grading
2. Surface texture differed:
    a. Yellow sand – smoother with less of a surface layer
    b. Red sand – textured and covered with a surface deposit
3. Chemical analysis
    a. Yellow sand – significantly higher percentage of Si (double)
    b. Red sand – slighter higher percentage of Fe and Al

Two comparative photos taken during the investigation are shown in Figures 3 a and b. Chemical composition of the layers of surface material on the sand particles was determined by comparing grey scales of polished discs using the backscatter detector.

Yellow	Red
(a) 200µm	(b) 200µm
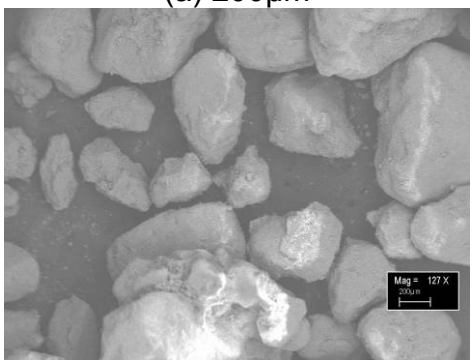	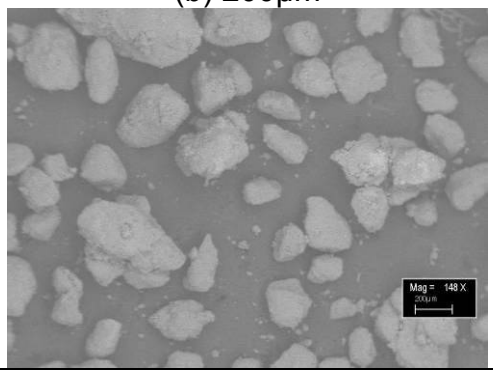

Figure 3: Electron microscope photos of yellow sand vs. red sand

During construction of the scaled pavement it was observed that the red sand dried and drained very slowly after being wetted to above optimum moisture content. It retained the moisture for an extended period of time. Soil suction was also high. These phenomena caused the sand to be water sensitive impacting on constructability of the pavement.

Wet, dry sieve and hydrometer analyses as well as particle size distributions from the sieve analysis were performed. The results in Table 3 indicate that the silt content of the red sand is five times more than the yellow sand (6.8 vs. 1.3). Furthermore the percentage passing 0.075 is three times more for the red sand. This confirms the results reported from the field testing by the contractor.

Maximum Dry Density (MDD) of the red and yellow sand were reported from construction records to be in the ranges of 1920 to 1950 kg/m3 and 1820 to 1850 kg/m3 respectively. It was concluded that these differences in the materials were the cause for the difference in strength values found with the two types of sand.

Table 3: Summary of hydrometer tests results

	Fraction Name	**Red Sand %**	**Yellow Sand %**
Fraction Size	Coarse Sand	15.3	61.8
2.0 mm > % > 0.425 mm	Fine Sand	72.8	32.9
0.425 mm > % > 0.05 mm	Silt	6.8	1.3
0.05 mm > % > 0.005 mm	Clay	5.1	4.0
0.005 mm > %	Silt + Clay	11.9	5.3
0.05 mm > % > 0.005 mm	% Passing 0.075	14.0	5.3

Strength and related tests

Extensive testing was done in Stellenbosch (Masondo, 2005) (de Vos 2007). The tests included the following:

- Indirect Tensile Strength (ITS)
- Unconfined Compression Strength (UCS)
- Shear Split Test (SST)
- Semi-circular bending strength (SCB) [subsequently discont]
- Three point bending [subsequently discont]
- Tensile strain-at-break ε_b
- Insitu Dynamic cone penetrometer measurements (DCP)

Tests were conducted on laboratory compacted briquettes. Cored specimens (100 mm diameter) from the full scale and laboratory scaled test sections were also tested to determine the one and a half year strength of in-situ pavements constructed and cured according to current construction practice. Extracts from the results are contained in Tables 4, 5 and 6. Supplementary to the above tests the change in stiffness with increased number of load applications was measured to monitor structural performance. The Portable Seismic Pavement Analyser (P-SPA) was utilized for this purpose.

The shear split test was incorporated to assess material shear strength since interface distress between the HMA and CTB occurred in sections tested (see later). The shear split test comprises vertical splitting along the diameter of a 60 by 100 mm diameter specimen or core at a displacement rate of 50.8 mm per minute while monitoring the load applied. The shear split test method was developed by Lorio (1993, 1997). The testing rig was modified and methodology adapted for use in the Materials Testing Machine (MTS), the test setup is illustrated in Figure 4. The following discussion relates to the strength and related test results.

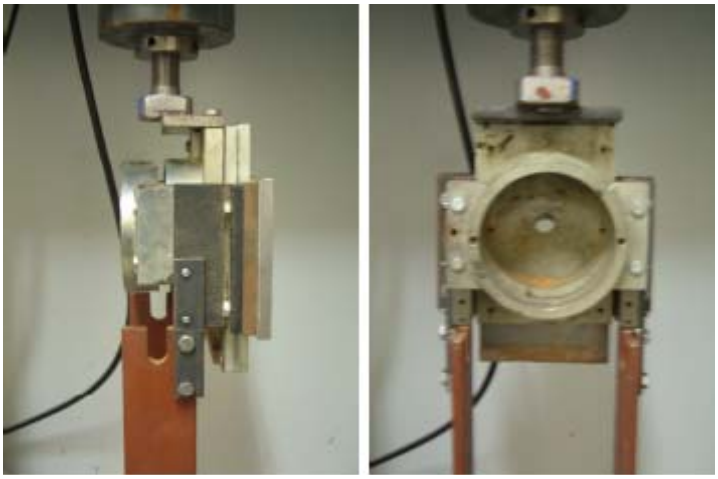

Figure 4: Shear split test setup (side and frontal view)

Table 4: Summary of material test results conducted on laboratory prepared specimens

SAND TYPE	BINDER	ITS 7 DAY		ITS 28 DAY		UCS 28 DAY		SHEAR 28 DAY	
		kPa	COV	kPa	COV	kPa	COV	kPa	COV
Red	3 % CEM	200	8	290	15	1500	23	270	9
Red	5 % CEM	310	11	540	8	2220	14	540	3
Red	7 % CEM	350	15	550	16	2500	25	650	11
Red	2.5 % CEM 2.5 % Lime	130	15	200	13	880	21	400	1
Red	3.5 % CEM 3.5 % Lime	210	13	450	15	1490	23	470	12
Yellow	7 % CEM	390	18	870	5	3600	8	690	11

*COV - Coefficient of Variation = Standard Deviation / Average x 100

Table 5: Summary of test results obtained from tested full-scale field test section cores at an age of 1.5 years

SAND TYPE	BINDER	ITS		UCS	SHEAR
		TYPE 2	TYPE 1		
		kPa	kPa	kPa	kPa
Red	3 % CEM	-	-	-	-
Red	5 % CEM	360	596	4879	270
Red	7 % CEM	680	-	5190	360
Red	2.5 % CEM 2.5 % Lime	938	-	4720	-
Red	3.5 % CEM 3.5 % Lime	-	-	-	-
Yellow	7 % CEM	1094	-	3866	370

From comparison with SAMPD standards (TRH 14, 1985) the CTB material conforms to C2 and C3 material class standards according to ITS and UCS results respectively. However, it should be noted that the reference standard relates to G5 or G6 material as CTB material which is of course different in structure and composition from the Mozambiquen sand.

Table 6: Summary of ITS test results of cores taken from scaled laboratory test sections at an age of 1.5 years

SAND TYPE	BINDER	HMA		SEAL	
		kPa	COV	kPa	COV
Red	3 % CEM	-	-	-	-
Red	5 % CEM	350	10	-	-
Red	7 % CEM	1700	15	1000	17
Red	2.5 % CEM 2.5 % Lime	550	29	-	-
Red	3.5 % CEM 3.5 % Lime	680	10	-	-
Yellow	7 % CEM	530	2	-	-

Tensile and shear strengths obtained from laboratory compacted and specimens cored from full-scale and scaled test sections do not correlate well. This was attributed to differences in the mixture quality, compaction and curing methodology and environmental circumstances. Field sections were subjected to environmentally induced distress and traffic loading of paving and surface compaction machinery during early life strength gain.

Compressive strength results compare favourably by indicating increased compressive capacity with ageing. It would appear that the compressive strength of the field CTB is less susceptible to early age damage caused by heavy loading of the construction equipment than the shear and tensile characteristics. The results further indicate that the retarded initial trength gain of the cement – lime blends relative to the cemented material increased with time to surpass the materials stabilized with cement only. The above results compare favorably with other reported studies (Melis et al. 1978 and Croney and Croney, 1991).

ITS strengths of lime stabilized granular pavement materials were studied in-depth by Melis et al (1978). One of the outcomes was the relationship between UCS, Modulus of Rupture (MR) and ITS It was concluded that MR was about 50 percent greater than ITS strength. This correlation was then applied to the ITS values measured on the Mozambican sands, with a further correction to allow for ageing after research on stabilized materials by Croney and Croney (1991) [Figure 13.3]. The results were subsequently used to determine the ratio of tensile stress under loading relative to tensile strength at failure to adjudicate fatigue performance [Figure 13.9 Croney and Croney (1991)].

CONSTRUCTION OF FULL-SCALE FIELD TEST SECTIONS

The pavement structure comprised insitu sandy subgrade, 150 mm imported red sand subbase, 150 mm CTB and a surfacing of HMA or a double seal. Two different methodologies for compaction of the CTB were specified:

- Type 1 : Compation by vibrating padfoot roller for six passes followed by pneumatic tyre rolling for four hours. Compation had to be completed six hours after mixing of the stabilising agent had started.
- Type 2 : Compation by vibrating padfoot roller for six passes followed by pneumatic tyre rolling for six passes only. Compation had to be completed three hours after mixing of the stabilising agent had started.

Construction Type 1 is conventionally used by contrators to attain the high design densities prescibed – 97 percent of Modified AASHTO (MAASTHO). This requires a relatively long compaction period resulting in the break down of initial cementing action by the heavy construction equipment. Over compaction and destruction of the surface of the base layer occurs with some rollers when the number of passes exceeds a critical level. From construction experiments the steel drum roller caused surface shear while the pneumantic tyre roller has a kneading action on the fresh CTB material and smooth surface finish. Figure 5 depicts the test arena adjacent to the existing rehabilitated highway EN1. The results of the respective laboratory tests for material characterization of the respective test sections are shown in Table 7. Construction was completed in June 2005.

The protocol for full-scale trafficking with the MLS10, was based on the performance of the respective MMLS3 test sections. Maximum tensile stress at the underside of the scaled CTB pavement was calculated and compared to the maximum tensile stress under the full-scale pavement. The expected full-scale trafficking yielding similar distress, was then calculated on the basis of a “fourth power law” of 4.2. Material characteristics and test conditions were assumed similar. For example, the 5% CTB the MMLS3 trafficking was terminated at 1.3 million load applications and the expected full-scale performance was found to be 100 000 using 60kN loads. For the 7 percent CTB the expected full-scale yielded 230 000 60 kN loads. It was concluded that 1 million 60 kN load applications would

be sufficient for realistic diagnostic analyses. For environmental conditioning of the full scale tests, trafficking was alternated between 200 000 ambient dry and 50 000 wet load cycles with water sprayed onto the pavement surface (de Vos, 2004). Channelized loading was applied with no lateral wander.

FULL-SCALE AND SCALED FIELD APT BY MEANS OF MLS10 AND MMLS3

During this phase of the study the following data was collected:

- Dynamic surface deflections during trafficking using an extended Benkelman Beam in lieu of Falling Weight Deflectometer measurements
- Seismic stiffness using the PSPA
- Surface deformation by means of a electronic profilometer
- Surface cracking and related distress through photos, diagnostic, trenching and coring
- Diagnostic trenching after completion of traffic loading in conjunction with coring

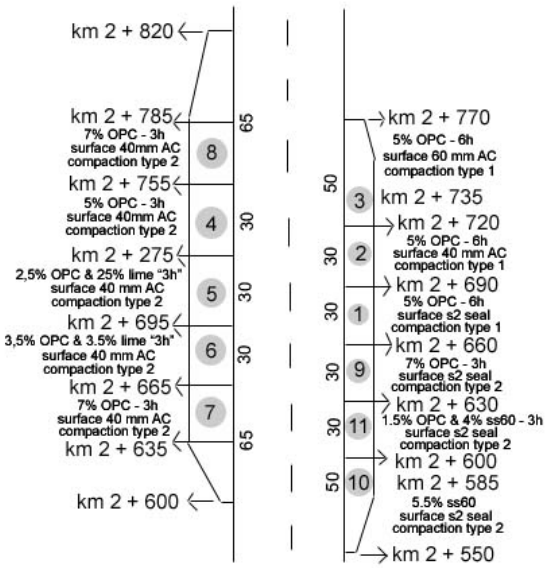

Figure 5 Plan view of Test Sections constructed in June 2005

EVALUATION OF PAVEMENT PERFORMANCE TO ESTIMATE THE FULL-SCALE PERFORMANCE CHARACTERISTICS OF THE TEST SECTIONS.

Pavement behaviour at different stages during performance phases under trafficking

were similar for the tested sections. The pavement surfaces started to roll dynamically in wave form under loading tyres, with deflections visible with the naked eye when de-bonding occurred. Six comprehensive MLS10 tests were completed. The details are shown in Table7.

TABLE 7 Control test results for Constructed Full-Scale MLS Test Sections

Section No.		1	2	3	4	5	6	7	8	9	10	11
Surfacing		Double Seal	40mm AC	60mm AC	40mm AC	40mm AC	40mm AC	40mm AC	40mm AC	Double Seal	Double Seal	Double Seal
Stabilized with		5% CEMII 32.5			5% CEMII	2.5% CEMII 2.5% L	3.5% CEMII 3.5% L	7% CEMII	7% CEMII	7% CEMII	5.5% SS60	CEMII 1.5/4.0 SS60
MATERIAL SOURCE		Palmeira - Red			Red	Red	Yellow	Y	Red	Red	Red	Red
SIEVE ANALYSIS												
19.0mm					100				100		100	
13.2mm					98	100	100		96	100	98	100
4.75mm		100			94	99	98	100	96	99	98	96
2.0mm		94			85	96	95	96	92	98	97	92
0.425mm		81			79	84	83	44	79	92	81	83
0.075mm		7			15	11	16	6	6	19	15	16
GM		1.81			1.21	1.09	1.06	1.54	1.23	0.91	1.07	1.09
PI		NP			NP	NP	NP	NP	NP	NP	NP	NP
LINEAR SHRINKAGE		0.0			0.0	0.0	0.0	0.0	0.0	0.0	0.0	0.0
MOD AASHTO												
MDD		1956			2025	2012	1887	2022	2023	1948	2069	1951
OMC		10.4			9.0	9.8	10.8	8.4	9.1	9.7	7.8	9.8
MOULDING MOISTURE(%)		10.4			8.7	9.8	11.3	8.2	9.1	9.8	8	11.8
MDD)		97.6			94.1	94.6	102.1	96.7	94.8	96.8	95.4	101.0
ITS												
ITS (KPa)		280.00			600.00	550.00	620.00	300.00	610.00	490.00	280.00	80.00
Avg. Compaction		100.3			99.6	100.2	99.1	98.7	98.6	99.7	97.8	99.1
UCS												
PR	COMP %	88.8			89.0	89.2	89.3	89.7	88.7	86.8	91.1	89.8
	UCS(MPa)	0.55			1.56	1.22	1.27	1.05	1.05	0.66	0.43	0.74
MD	COMP %	98.8			99.7	100.3	98.2	98.8	98.4	99.5	98.1	99.0
	UCS(MPa)	2.42			2.33	3.94	2.38	1.90	3.81	3.53	1.45	0.84

Table 8: Summary of MLS10 Tests

Section	8a	4a	5a	5b	8b	4b	8c	7
Stabilizing Binder	7 % Cem	5 % Cem	2.5% C 2.5% L	2.5% C 2.5% L	7 % Cem	5 % Cem	7 % Cem	7 % Cem
Sand for CTB (150mm)	Red	Red	Red	Red	Red	Red	Red	Yellow
Surfacing (40mm)	HMA	HMA	HMA	HMA	HMA	HMA	HMA	HMA
Axle load X 1000 applications	50	330	100	1,080	84,5	150	730	1 050
Axle Load kN	60	60	60	60	60	70	70	70

MONITORING OF RESPONSE AND PERFORMANCE DURING FIELD APT

Dynamic deflection performance

The dynamic defections measured with the MBB were used in lieu of FWD tests. Geometric features of the deflection bowl were determined relative to FWD norms. Results for 70 kN are shown in Figure 6d. If deflection bowls are transposed to 40kN wheel loads the traffic life is likely to extend well beyond 10 million axles (TRH12 (1986). This compares favourably with the other performance predictions that were established. TRH12 (1986) is of course based on granular and not sandy materials.

(a) MBB set-up under the MLS10

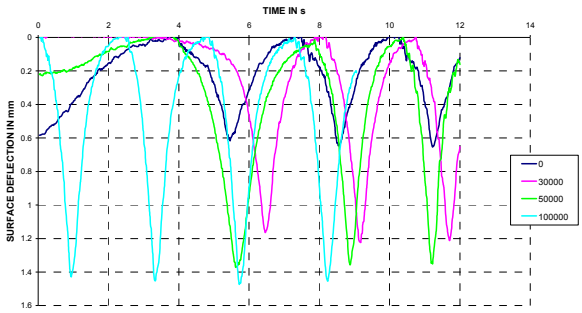

(b)Deflection change as applications increase

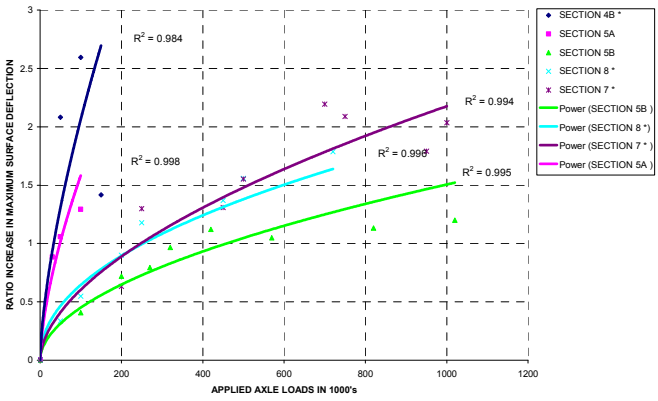

(c) Peak deflections for different pavement sections as load applications increase

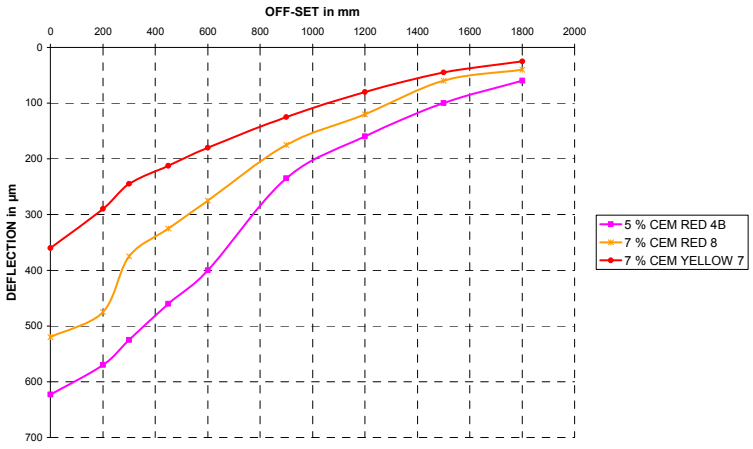

(d) Deflection bowls of sections 4B, 7 and 8 under 70kN wheel loads

Figure 6 Graphic depiction of dynamic deflection results under moving wheel loads

Seismic stiffness changes during APT using P SPA measurements

Seismic stiffness monitoring was conducted with the PSPA device developed by Nazarian et al. (1993). The operating principle of the PSPA is based on generating and detecting stress waves in a medium. The Ultrasonic Surface Wave (USW) interpretation method (Nazarian et al., 1993) is used to determine the modulus of the material. Surface waves (or Rayleigh, R-wave) contain two-thirds of the seismic energy. Accordingly, the most dominant arrivals are related to the surface waves making them the easiest to measure. This method utilizes the surface wave energy to determine the variation in surface wave velocity (modulus) with wavelength (depth). The variability of tests results with PSPA is less than 3% without moving the device and around 7% when the device is moved in a small area (Celayn et al. 2006).

The surface wave velocity, VR, is converted to modulus, E, using:

$$E = 2\,[\rho\,(1.13 - 0.16)V_R]^2\,(1 + v) \qquad (3.1)$$

Where:
E = modulus
V_R = velocity of surface waves
ρ = mass density
v = Poisson's ratio

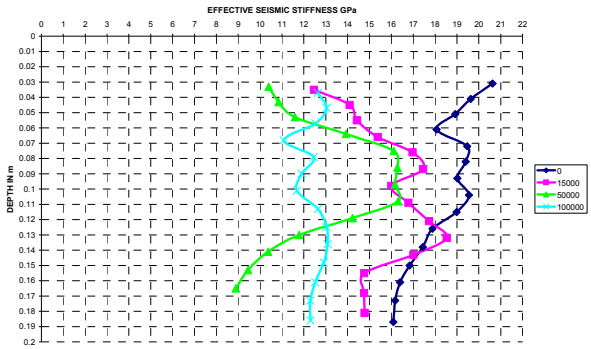

Figure 7 Typical seismic stiffness vertical profiles with axle load application

The stiffness of the pavement structure and more particularly the upper 200mm was measured at regular intervals during trafficking. Measurements were taken in longitudinal and transverse directions, relative to the wheel path. Figure 7 shows desperion curves with increase in axle loading to illustrate the relative reduction in the shear wave speeds, seismic modulus, with increased pavement distress. In general the change in longitudinal stiffness was more than that in the transverse direction.

LAYERED EXTRACTION OF PSPA RESULTS

From the initial MML3 laboratory testing different mechanisims of failure occured in certain particular pavement zones. Interface distress in the form of shear failure between the surfacing and the CTB occured on the top of the CTB. Horisontal shear planes were found in the middle of the CTB layer. Flexural cracking in the longitudinal and transverse directions starts at the bottomof the layer and progress with traffic loading to the top. The bottom of the CTB crushes into smaller pieces when pavement life nears its end. Diagnostic trenching after completion of traffic loading confirmed this phenomenon (see Figure 12a under synthesis discussion).

Subsequently wavespeed – frequency dispersion curves were analysed accordingly. The CTB layer were partitioned into thee zones the Top, Middle and Bottom comprising of the top 25 mm, 50mm and 75 mm of the 150 mm CTB layer. The stiffness reduction methodology was developed by the de Vos (2007) for the characterization of specific pavement zones based on their respective structural performances. The dispersion curves were reduced by averaging of the datapoints occuring in or on the boundry of each respective zone, Top, Middle and Bottom. Direct ratios were calculated between initial untrafficked and measurements taken as traffic accumulated for each zone at each measurement location in each of the two directions of measurement.

PAVEMENT STIFFNESS PERFORMANCE UNDER FULL-SCALE TRAFFICKING

In general the change in longitudinal stiffness was more than that in the transverse direction. Figure 8a – d illustrates the stiffness performance. Figure 8 (c) illustrates the performance of the bottom zone of CTB at the worst performing position of each tested section in the longitudinal direction. Performance of this zone and in this direction was the worst.

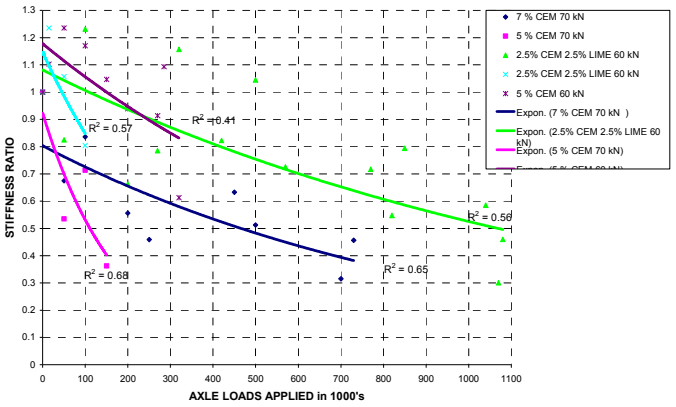

(a) Comparative longitudinal stiffness performance top of CTB

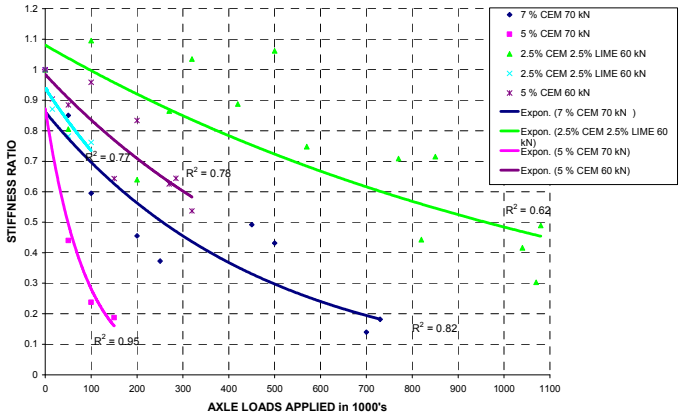

(b) Comparative longitudinal stiffness performance bottom of CTB

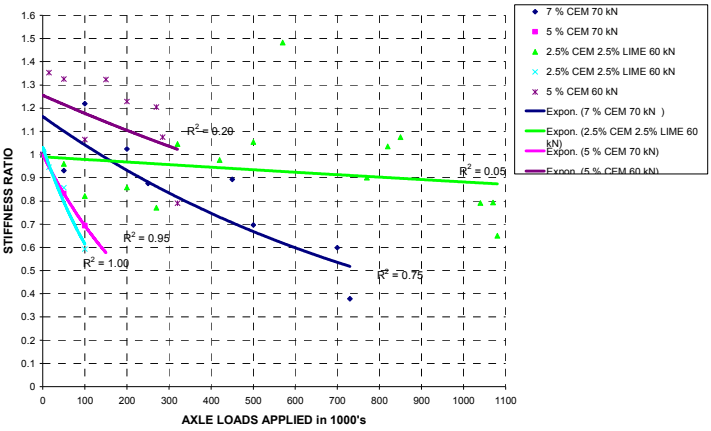

(c) Comparative transverse stiffness performance for top of CTB

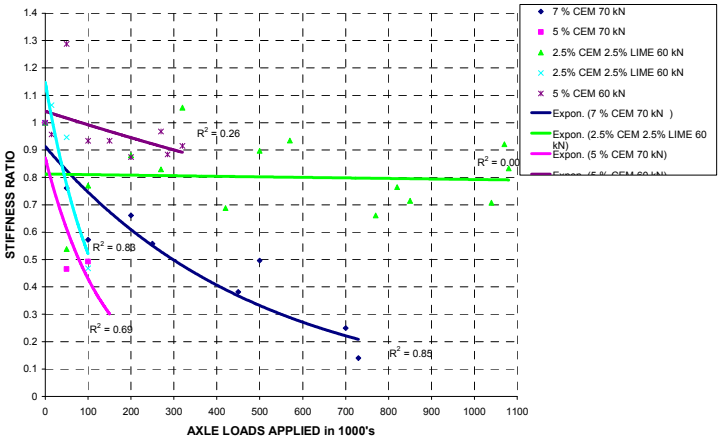

(d) Comparative transverse stiffness performance bottom of CTB

Figure 8: Extracts from longitudinal and transverse PSPA stiffness results

Surface deformation

Rutting of the surface was limited and attributed to the interface distress and pulverizing of the CTB as well as the removal of the loose material pumped out through the surface cracks. Where failure occurred in the layer, the surface naturally deformed much more.

Surface crack formation

Cracking was monitored intermittently by visual inspection and photographic recording. Typical isometric views to illustrate crack growth phenomenon of Section 4A are shown in Figure 9. Note pumping and longitudinal cracks in left wheel track at 320k load applications.

Cracks diagonal to and on the outer edges of the wheel track and transverse cracks in-between the wheels were first to appear. Diagonal cracks resulted from longitudinal in-plane shoving of the HMA through in-plane horizontal shear forces and subsequent interface distress between the HMA and CTB. With increased traffic loading these cracks propagate across the wheel track in a direction perpendicular to it connecting with the transverse cracks formed in-between the wheels. This resulted in a complete transverse surface crack. Longitudinal cracks would start to form under the tyres interconnecting with the transverse cracks to form a crocodile cracking pattern.

(a)Transverse shear crack initiation at 270 000 60 kN load applications - Section 4

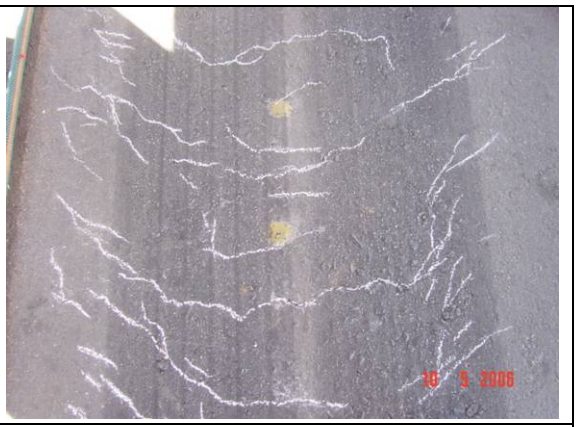

(b)Transverse propagation of shear cracks at 285 000 60 kN load applications - Section 4

(c) Continuous transverse cracks and longitudinal cracks after 320 000 60 kN Section 4

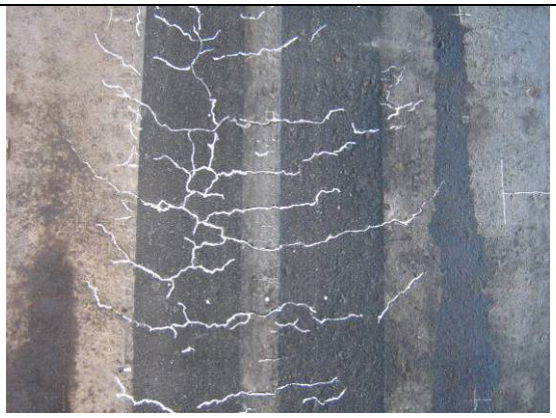

(d) Plan view of cracking pattern after 1 million 70 kN load applications- Section 7

Figure 9 Extracts from photographic records of crack formation under trafficking

Diagnostic evaluation through trenching

Diagnostic trenches 1000mm x 500 mm were made across selected wheel paths after completion of trafficking to investigate distress and failure mechanisms. Interface shear between the HMA and CTB layers took place under loading. Shear planes generally formed under the prime impregnated CTB surface. In-plane longitudinal displacement of the HMA was also recorded. Shear marks and smoothed shear surfaces were observed on both the HMA and CTB contact planes.

Longitudinal and transverse flexural cracks were observed. The pavement structure was fractured when the stiffness had reduced by 50 percent. It was also apparent that the fractured CTB blocks had experienced horizontal shoving of the HMA as trafficking progressed. From the test conducted on Sections 8 and 7 it was evident that the structure was more fractured when the stiffness ratio had significantly dropped to below 0.5 e.g. 0.2 – 0.3. With increased traffic loading the fracturing of the CTB progressively increased, reducing the particle size to smaller fractions with the smallest particles at the bottom.

Horizontal shear planes were found about one third from the top of the CTB. In the lower cement stabilized bases trafficked up to a stiffness loss of 50 percent, these shear planes were found to connect the bottom up longitudinal cracks at this depth. In the bases trafficked to a more severe state of distress it was found that the shear plane had propagated laterally in the CTB structure.

Section 8 was trafficked to a stiffness ratio as low as 0.2 when the pavement had deteriorated dramatically. Deep rutting occurred, severe pumping took place. The particle fractionation and loss of material through pumping lead to the deep rutting as well as shear failure of the asphalt on the edges of the wheel track.

It was found that two types of distress could develop simultaneously on the same pavement section. This was the case in Section 8. At the far end of the section the distress was as three types discussed above. In contrast, at the start of the section the CTB had not shattered, but the HMA had deformed due to shoving of the asphalt material longitudinally as well as transverse shear adjacent to the wheel.

In all cases the distress in the bottom of the CTB was similar in relation to the relative reduction in stiffness in both extent and orientation. It is of course important to remember that trafficking had been done without lateral wander. The similarity of the distress between the full-scale and the laboratory scaled pavements is apparent from the performance of the sections. Section 7 proved to be the best in terms of performance against initial expectations. The findings are also in accordance with the laboratory S/V results.

(a) Underside of HMA - section 8

(b) Top of CTB – section 8

Figure 10 Extract from photographic records of diagnostic findings through trenching

SYNTHESIS OF SCALED AND FULL-SCALE APT PERFORMANCE FINDINGS

Manifestation of distress followed a pattern that had been identified in MMLS3 laboratory study on scaled pavements (de Vos et al. 2007). The postulated failure mechanisms are based on the findings presented above.

Interface distress between HMA and CTB contact surfaces

Asphalt surfacing exhibited in-plane horizontal longitudinal displacement at the interface. This resulted in diagonal shear fractures (cracking) on the sides of the wheel path. This phenomenon is clearly related to shear bond between asphalt surfacing and CTB. Continued traffic loading leads to pulverizing and distress

aggravates when water infiltrates during load trafficking. Pulverized material migrates through cracks by means of pumping action. Initial surface rutting relates to removed pulverized interface material. Diagnostic trenching exhibited clear evidence of this distress. Some typical details are depicted in Figure 10 a and b. In the later stages of pavement life the HMA shears off completely and the whole pavement experiences a dynamic bow wave under trafficking loads. The bow wave was so active that it was visible to the naked eye.

Longitudinal and transverse flexural cracking

Bottom-up transverse and longitudinal flexural cracking of the pavement was the primary mechanism of CTB structural failure. See Figure 12a and b. Reductions in stiffness ratios were found to be greatest in the bottom pavement zone for all pavements.

Shear plane formation in the CTB

A secondary structural mechanism of failure is the occurrence of a horizontal shear plane in the CTB. This plane was generally found to occur in the middle of the combined HMA-CTB structure (100 mm from the top). This position is also one third of the CTB thickness from the top thereof (50 mm). This plane links the two longitudinal cracks and forms a 'shear box'. (see Figures 12a and b. A similar mechanism was found with the scaled laboratory testing of this material (de Vos et al. 2007).

A linear elastic shear stress analysis was done with Bisar 3.0 (Shell, 1998) to simulate and investigate this phenomenon. Two pavements model were analyzed for evaluation of the shear stress distribution in the pavement before and after interface distress. The pavement structure representing the pavement before interface distress had a full friction interface between the HMA and CTB. The second pavement model had a 10 mm layer in between the HMA and CTB with the same attributes than the sub base, to simulate the sheared and pulverized interface. Shear stress pavement profiles for the 'Bonded' and 'Unbonded' scenarios are illustrated in Figure11. The plots illustrate that maximum shear stress is initially at the HMA-CTB interface. After failure thereof, the maximum shear stress is found in the middle of the combined pavement structure, 100 to 125 mm from the top, hence formation of the horizontal in-plane shear crack. Table 9 shows working stress to strength ratios for both the interface and shear plane mechanisms.

Table 9: Stress to strength ratios for the interface and shear plane failure mechanisms

Condition	HMA - CTB Interface Mechanisms	CTB Mid Layer Shear Plane Mechanisms
5% / 60 kN	1.09	0.90
5% / 70 kN	1.12	0.97
7% / 70 kN	0.82	0.75

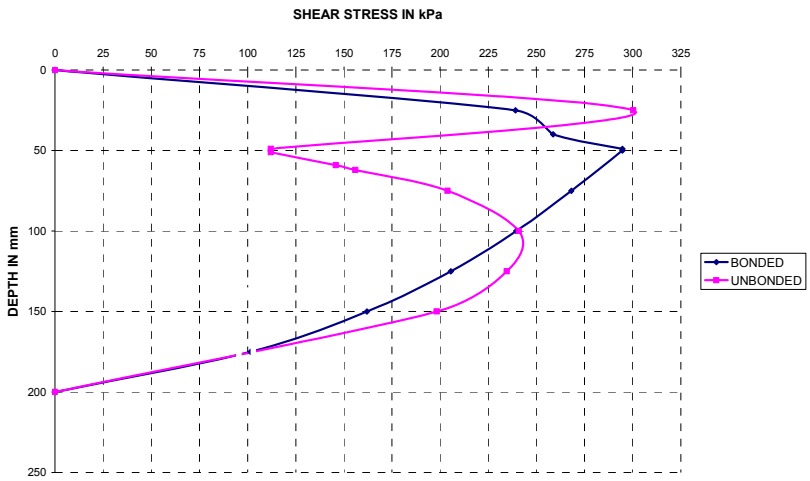

Figure 11: Shear stress plots for 5 percent CTB under 60 kN axle load

(a) Front view – section 4B- note horizontal shear plane and longitudinal cracks

(b) Plan view – section 4B- note longitudinal and transverse cracks

(c) Progressive phases of failure-scaled 3 percent CTB section.

(d) Shear plane on neutral axis of 50mm scaled 3 percent CTB with seal,

Figure 12 Photographic depictions of distress development under trafficking

From the illustrated shear stress plots and ratios presented, it was concluded that the interface distress occurs first followed by shear plane formation. The high stress to strength ratios for the 5 percent CTB sections further indicate why the interface distress initiates much earlier relative to the gradual stiffness loss at the bottom part of the base. A comparison between the 5 and 7 percent cement treated sections' ratios indicate why the shear crack formation for the higher cemented sections start later in the pavement life (after 50 percent base stiffness loss).

Diagnostic evaluation of Sections 4B, 8 and 7, that were tested with higher loads to reduce stiffness values as low as 30 to 20 percent of the initial, showed that these CTB blocks were fractionized further into much smaller particles. At that stage of pavement life, severe lateral asphalt movement had taken place resulting in wide transverse and diagonal cracks (1 – 2 mm). Fine crushed material was pumped out; this resulted in vertical shear of asphalt as there was less supporting base material left beneath the wheel tracks. Subsequent significant increases in rutting were also observed under these conditions. Maximum surface deflections of 2.8 to 4 times that of the initial untrafficked deflections were measured. Relative increases in the deflection ratios are smaller from 50 to 80 percent stiffness loss as the pavement loses structural integrity and ability to respond elastically under loading. Figure 13 illustrates this phenomenon.

The various distress modes causing the disintegration of the pavement structure were found to occur in different sequences depending on the structure of the pavement and the strength of the materials. For the higher strength cemented bases the interface distress occurred later in pavement life relative to the base stiffness loss than the lower strength cement treated bases. This is ascribed to the stress strength ratio under traffic loading at the pavement interface.

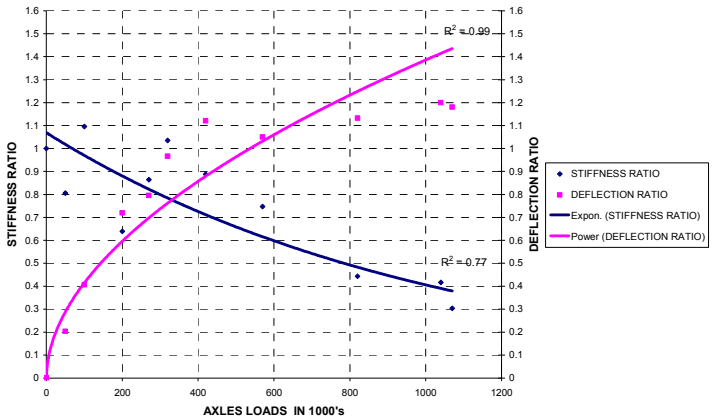

Figure 13 Stiffness – Deflection performance of 2.5 % cement and 2.5 % lime stabilized red base material under 60 kN axle loading

CONCLUSIONS

The following noteworthy aspects of the performance of the CTB were concluded:

- Bottom-up transverse and longitudinal flexural cracking of the pavement was the primary mechanism of CTB structural failure.
- Horizontal shear planes manifest as secondary CTB structural mechanism of failure in the CTB.
- Distress due to delamination between surfacing and the CTB was found to relate to the shear stress and bond strength. Asphalt surfacing exhibited in-plane horizontal longitudinal displacement. This resulted in the observed diagonal shear fractures on the outer edges of the wheel path.
- Response and performance of full-scale pavement structures and model pavements in the laboratory were compatible with manifestation of similar failure mechanisms. Difference in surface distress was attributed to the difference in contact stresses.
- Pulverized material migrates through cracks by means of pumping action leading to distress of the surfacing.
- The axle loads of 60 kN and subsequently 70 kN, provided insight into distress mechanisms and information pertaining to performance.
- With the 7% CTB, de-bonding distress occurred after the PSPA stiffness had reached 0.5. This improved performance of the pavement.

ACKNOWLEDGEMENTS

The authors gratefully acknowledge permission to publish the findings from the research reported in this paper. It was done as an integral part of project

206/CON/ES/DEN/2003 for the ANE. Funding was sponsored by the World Bank. The opinions expressed by the authors do not necessarily reflect those of the sponsors.

REFERENCES

Celayn, M, Nazarian, S 2006. Seismic Testing to Determine Quality of Hot-Mix Asphalt, CD-Rom Proceedings 85th Annual TRB Meeting, Washington, D.C.

Croney, D and Croney, P 1991. The Design and Performance of Road Pavements; McGraw-Hill International Series in Civil Engineering, 2nd Edition.

de Vos, E R 2004. Development of a Accelerated Laboratory Testing Protocol for Cement Stabilized Base Layers using the Third Scale Model Mobile Load Simulator; B.Ing Thesis, University of Stellenbosch, November

de Vos, E R 2007. Performance Characterizaion of Cement Treated Sand Base Material of Mozambique, M.Ing Thesis, University of Stellenbosch, April

de Vos, E R, Hugo, F, Strauss, P J, Prozzi, J A, Fults, K W, Tayob, H 2007. Comparative Scaled MMLS3 Tests vs. Full-Scale MLS10 Tests in Mozambique; CD-Rom Proceedings, 86th Annual TRB Meeting; Washington D.C.

Lorio, R,1994. The Asphalt Shear Box Test, B.Eng Thesis, Univ Stellenbosch.

Masondo, PT, 2005. Testing Parameters for Cement Treated Base Courses; Project submitted for fulfilment of BEng Degree; Faculty of Engineering, University of Stellenbosch; November

Melis, L M, Meyer, A H and Fowler, D W 1985. An Evaluation of Tensile Strength Testing; Research Report 432-1F, Centre for Transportation Research, The University of Texas at Austin, November.

Nazarian, S, Baker, M R, and Crain, K 1993. Fabrication and Testing of a Seismic Pavement Analyzer; SHRP Report H-375. SHRP, National Research Council, Washington, D.C.

Shell International Oil Products BV 1998. *Bisar 3.0* (computer programme).